

An efficient mixed variational reduced order model formulation for non-linear analyses of elastic shells

D. Magisano¹ K. Liang² G. Garcea¹ L. Leonetti¹ M. Ruess^{3*}

¹ *Dipartimento di Ingegneria Informatica, Modellistica, Elettronica e Sistemistica, Università della Calabria 87036 Rende (Cosenza), Italy*

² *School of Aeronautics, Northwestern Polytechnical University, Xi'an 710072, PR China*

³ *School of Engineering, University of Glasgow, Glasgow G128LT, United Kingdom*

SUMMARY

The Koiter-Newton method had recently demonstrated a superior performance for non-linear analyses of structures, compared to traditional path-following strategies. During a predictor step, the approach constructs a reduced order model based on Koiter's asymptotic post-buckling theory and combines its solution with a number of Newton iterations in a corrector phase to regain the equilibrium of forces.

In this manuscript, we introduce a robust mixed solid-shell formulation to further enhance the efficiency of stability analyses in various aspects. We show that a Hellinger-Reissner variational formulation facilitates the reduced order model construction omitting an expensive evaluation of the inherent fourth order derivatives of the strain energy. We demonstrate that extremely large step sizes with a reasonable out-of-balance residual can be obtained with substantial impact on the total number of steps needed to trace the complete equilibrium path. More importantly, the number of corrector steps involving Newton iterations of the full system is drastically reduced to a few iterations per step thus revealing the true strength of the proposed formulation. We study a number of problems from engineering and compare the results to the conventional approach in order to highlight the gain in numerical efficiency for stability problems.

Copyright © 2017 John Wiley & Sons, Ltd.

Received ...

KEY WORDS: reduced order model, buckling, geometrically non-linear analysis, solid-shell, mixed formulation.

CONTENTS

1	Introduction	2
2	Review of the Koiter–Newton approach	3
2.1	Construction of the reduced order model	3
2.2	Koiter-Newton path-following analysis	6
3	Solid-shell concept and mixed formulation	6
3.1	Displacement-based solid-shell element	7
3.1.1	Kinematics	7
3.1.2	Discretization aspects	8
3.1.3	Statics	8

*Correspondence to:

†E-mail: martin.ruess@glasgow.ac.uk

3.1.4	Displacement-element contributions to the third order form governing equations	9
3.2	Mixed solid-shell element	10
3.2.1	Mixed-element contributions to the third order form governing equations	11
4	Numerical tests	12
4.1	U-shape cantilever beam	12
4.2	Lipped channel column	15
4.3	Laminate composite cylinder subjected to axial compression	15
4.4	Thin-walled frame	18
5	Summary, Conclusions & Outlook	20

1. INTRODUCTION

Classical path-following strategies as used in the numerical analysis of buckling phenomena of thin-walled structures operate on a linearized form of the non-linear governing equations of the deforming structure. A predictor step followed by a number of corrector iterations is used to trace the entire load-displacement equilibrium path in a step-by-step manner [1]. The linearized equations allow for linear predictor steps only, tangential to the equilibrium path, which results in a substantial number of steps required to capture the full non-linear structural response. Furthermore, linear predictors easily fail to detect bifurcation along the equilibrium path unless a very small step size is adopted. Over the years, a number of asymptotic methods based on Koiter's post-buckling theory [2] have been developed to provide a failsafe analysis method at significantly reduced costs [3, 4, 5, 6, 7, 8, 9]. The Koiter method constructs a reduced order model based on a second order asymptotic expansion using the path tangent and a few buckling modes. The method reduces the large number of equations needed to model accurately the elastic buckling behavior of shells to a few nonlinear equations representing the modal amplitudes and the load factor of the deformed structure [10, 11].

Recently, a novel Koiter-Newton approach has demonstrated successfully a reliable and accurate prediction of the buckling phenomena of thin-walled structures [12, 13, 14]. The main idea of this approach is the use of Koiter's method as a non-linear predictor within the framework of a path-following strategy. The asymptotic characteristics of the proposed predictor step allows for significantly larger step sizes at reduced out-of-balance residual forces, the latter having a positive effect on the overall effort of the corrector phase. The method allows to trace the entire equilibrium path and to handle reliably snap-back and snap-through phenomena [15]. In an extended version, the method provides a bifurcation indicator based on the constructed reduced order model which enables to trace the corresponding bifurcation branches [16]. The method has proven to be a robust and computationally efficient solution approach though the corrector phase cannot fully profit from the reduced order model and requires a number of Newton iterations based on the full model. In the past, it has been observed in several studies that mixed (stress and displacement) finite elements show superior properties compared to pure displacement-based elements in the context of a standard Newton approach for non-linear analyses [17, 18]. In general, the mixed formulation allows for larger step sizes and requires less iterations to regain equilibrium as highlighted in [19] for beam elements. A more recent work [20] observed the beneficial convergence properties of mixed model formulations in a general context, extendible to displacement-based finite element formulations following the mixed integration points strategy proposed in [21]. The studies show that the evolution of the iterative displacement process is forced to satisfy the constitutive equations in each iteration and this constraint leads to a drop of the convergence rate. In contrast, the stress components in the mixed model are introduced as independent variables which only satisfy the discrete constitutive equations at convergence.

Focusing on a mixed model formulation, this paper combines the superiority of mixed elements in terms of convergence properties with the efficiency of the reduced order principles of the

Koiter-Newton approach. We exploit the direct prediction and correction of the stresses to minimize the number of Newton iterations of the corrector phase. The Koiter predictor constructs a *reduced order model* which requires derivatives of the strain energy up to the fourth order. Geometrically exact shell models [22] or co-rotational approaches [23, 24, 15] are suited formulations to achieve structural model objectivity. Both strategies make use of finite rotations which make the evaluation of the strain energy and its derivatives highly complicated and expensive. In [13] simplified kinematics were proposed to streamline the construction of the reduced order model at the price of reducing its range of applicability.

In this work, the Koiter-Newton method is implemented for a non-linear Cauchy continuum based on a Green-Lagrange strain measure and a solid-shell element interpolation [17, 25]. In this way, the construction of the reduced order model remains simple and favorable, maintaining a geometric exact strain measure. Furthermore, we adopt the Hellinger-Reissner variational principle in which the strain energy has only a third order polynomial dependence on the degrees of freedom while zeroing all fourth order strain energy variations. Thus, the reduced order model construction is simpler and faster [10]. We develop the mixed solid-shell element in the framework of the Koiter-Newton method and derive the governing equations and algebraic quantities needed for the context of the reduced order modeling. We verify our proposed model with a number of numerical tests, critically assessing its performance, its strengths and potential limitations. All numerical studies compare the proposed mixed model with the conventional displacement-based model, both showing a significant improvement compared with classical path-tracing methods.

The paper is organized as follows: in Section 2, we briefly recall the Koiter-Newton method and provide the governing equations for the construction of the reduced order model. In Section 3, a solid-shell model is introduced and extended to a mixed formulation providing the first, second and third algebraic quantities of the asymptotic extension. A number of numerical test for verification and validation of the proposed and implemented model is presented in Section 4 which includes benchmark tests and examples from engineering. Finally, we summarize the main findings and conclude the presented work in Section 5.

2. REVIEW OF THE KOITER-NEWTON APPROACH

In the following, we briefly recall the principles and properties of the Koiter-Newton approach. The method is capable to trace automatically the entire equilibrium path of a structure in a step by step manner. Each step involves the construction of a reduced order model at a known equilibrium state. The construction is based on Koiter's asymptotic theory on initial post-buckling stability [2] and used as a predictor within a path-following analysis. In a corrector step following each prediction, a few Newton iterations are used to reduce the residual error to a pre-defined equilibrium level.

2.1. Construction of the reduced order model

The non-linear behavior of an elastic body is analyzed, considering its state of equilibrium. Following a *Principle of Virtual Work*-formulation, the N governing non-linear equations of the discretized structure result in a set of algebraic equations:

$$\mathbf{R}(\mathbf{u}, \lambda) = \lambda \mathbf{f}^{ext} - \mathbf{f}^{int}(\mathbf{u}) = \mathbf{0} \quad (1)$$

where \mathbf{R} is the residual force vector, \mathbf{f}^{ext} represents the external load vector and λ is the load factor. The internal elastic forces \mathbf{f}^{int} are dependent on the vector of primal unknowns \mathbf{u} :

$$\mathbf{f}^{int} = \frac{\partial U(\mathbf{u})}{\partial \mathbf{u}} \quad (2)$$

where $U(\mathbf{u})$ is the strain energy of the structure.

In the Koiter-Newton approach, a reduced order model is established to approximate the equilibrium equations in the neighborhood of a known equilibrium state $(\mathbf{u}_0, \lambda_0)$ which is referred

to in the following as *nominal configuration*. Further, we denote an unknown configuration near the nominal configuration with (\mathbf{u}, λ) where:

$$\mathbf{u} = \mathbf{u}_0 + \Delta\mathbf{u}. \quad (3)$$

Here, the concatenation of unknowns \mathbf{u}_0 and $\Delta\mathbf{u}$, eq. (3), is assumed to be an addition. Considering beams and shells which take into account finite rotations, the concatenation will depend on the parametrization of the rotations [26].

The non-linear equilibrium (1) is approximated with a truncated Taylor series expansion up to the third order with respect to \mathbf{u} of the nominal configuration. The expansion terms follow from differentiation of the strain energy U up to the fourth order with respect to the unknown primal vector \mathbf{u} according to (1) and (2). The equilibrium modifies to:

$$\mathcal{L}(\Delta\mathbf{u}) + \mathcal{Q}(\Delta\mathbf{u}, \Delta\mathbf{u}) + \mathcal{C}(\Delta\mathbf{u}, \Delta\mathbf{u}, \Delta\mathbf{u}) + O(\|\Delta\mathbf{u}\|^4) = \Delta\lambda \mathbf{f}_{ext} \quad (4)$$

where \mathcal{L} is a linear form, \mathcal{Q} is quadratic form and \mathcal{C} is cubic. Regarding a conservative system, there exists a direct correspondence between the forms of order p in eq. (4) and a symmetric p -dimensional tensor, applicable to every component of the vector equation. Correspondingly, the linear, quadratic and cubic form of (4) can be expressed in terms of a two-dimensional, three-dimensional and four-dimensional tensor, respectively [27]. Furthermore, we use the relations $\Delta\lambda = \lambda - \lambda_0$ and $\mathbf{f}(\mathbf{u}_0) = \lambda_0 \mathbf{f}_{ext}$.

We use the Koiter-Newton method in the context of elastic shell buckling analyses considering structures with branching equilibrium paths. It is convenient to consider perturbation loads which excite neighboring states of equilibrium to allow the system to change from the primary to a secondary equilibrium path. An appropriate selection of perturbation loads is discussed in detail in [12]. Taking into account these loads, the third order form of the equilibrium equations (4) may be extended to consider multiple loading of the form:

$$\mathcal{L}(\Delta\mathbf{u}) + \mathcal{Q}(\Delta\mathbf{u}, \Delta\mathbf{u}) + \mathcal{C}(\Delta\mathbf{u}, \Delta\mathbf{u}, \Delta\mathbf{u}) + O(\|\Delta\mathbf{u}\|^4) = \mathbf{F}\phi \quad (5)$$

where the α -th column of \mathbf{F} is formed by the a perturbation load vector \mathbf{f}_α and where the vector ϕ represents the load amplitudes. The first column of \mathbf{F} is chosen to be the external load vector \mathbf{f}_{ext} with a corresponding first amplitude entry $\phi_1 = \Delta\lambda$. Further columns of \mathbf{F} are formed by sub-loads:

$$\mathbf{f}_\alpha = \mathbf{K}_\sigma \mathbf{v}_\alpha \quad \alpha = 2, \dots, m+1 \quad (6)$$

where m is a number of closely spaced buckling modes \mathbf{v}_α and \mathbf{K}_σ is the geometric stiffness matrix of a linearized buckling problem [12].

The equilibrium (5) forms a $m+1$ dimensional hypersurface for which the solution \mathbf{u} is approximated favorably by a series expansion. To this end, the equilibrium surface is parametrised in terms of generalised displacements $\xi = \{\xi_1, \dots, \xi_{m+1}\}$, and the displacement \mathbf{u} is expanded to the third order with respect to ξ_i :

$$\Delta\mathbf{u} = \mathbf{u}_\alpha \xi_\alpha + \mathbf{u}_{\alpha\beta} \xi_\alpha \xi_\beta + \mathbf{u}_{\alpha\beta\gamma} \xi_\alpha \xi_\beta \xi_\gamma + O(\|\xi\|^4) \quad (7)$$

where $\{\alpha, \beta, \gamma\} = 1, 2, \dots, 1+m$, and the Einstein summation convention is applied. The first order displacements \mathbf{u}_α define the tangent plane to the equilibrium surface at the approximation point. Additional first order displacements are generated by considering the additional imperfection loads of eq. (6). The second order displacements $\mathbf{u}_{\alpha\beta}$ and third order displacements $\mathbf{u}_{\alpha\beta\gamma}$ describe the interactions among first and second order displacement fields, respectively.

The equilibrium surface may be parametrised with an infinite number of choices for ξ . Here, the parametrization is chosen work-conjugate to the load amplitudes which results in the following orthogonality constraints:

$$\mathbf{f}_\alpha^T \mathbf{u}_\beta = \delta_{\alpha\beta} \quad (8)$$

$$\mathbf{f}_\alpha^T \mathbf{u}_{\beta\gamma} = 0 \quad (9)$$

$$\mathbf{f}_\alpha^T \mathbf{u}_{\beta\gamma\delta} = 0 \quad (10)$$

where $\delta_{\alpha\beta}$ is the Kronecker delta. Similarly, the load amplitudes ϕ are approximated by a series expansion to ensure consistency in the governing equations:

$$\phi = \bar{\mathcal{L}}(\boldsymbol{\xi}) + \bar{\mathcal{Q}}(\boldsymbol{\xi}, \boldsymbol{\xi}) + \bar{\mathcal{C}}(\boldsymbol{\xi}, \boldsymbol{\xi}, \boldsymbol{\xi}) + O(\|\boldsymbol{\xi}\|^4) \quad (11)$$

with $\bar{\mathcal{L}}$, $\bar{\mathcal{Q}}$ and $\bar{\mathcal{C}}$ being still to be determined, linear, quadratic and cubic forms.

Using (7) and (11) in the equilibrium (5) and equating the coefficients of the various powers of $\boldsymbol{\xi}$ to zero results in the following three linear relations:

$$\bar{\mathcal{L}}(\mathbf{u}_\alpha) = \mathbf{F} \bar{\mathbf{l}}_\alpha \quad (12)$$

$$\bar{\mathcal{L}}(\mathbf{u}_{\alpha\beta}) + \bar{\mathcal{Q}}(\mathbf{u}_\alpha, \mathbf{u}_\beta) = \mathbf{F} \bar{\mathbf{u}}_{\alpha\beta} \quad (13)$$

$$\bar{\mathcal{L}}(\mathbf{u}_{\alpha\beta\gamma}) + \frac{2}{3}(\bar{\mathcal{Q}}(\mathbf{u}_{\alpha\beta}, \mathbf{u}_\gamma) + \bar{\mathcal{Q}}(\mathbf{u}_{\beta\gamma}, \mathbf{u}_\alpha) + \bar{\mathcal{Q}}(\mathbf{u}_{\gamma\alpha}, \mathbf{u}_\beta)) + \bar{\mathcal{C}}(\mathbf{u}_\alpha, \mathbf{u}_\beta, \mathbf{u}_\gamma) = \mathbf{F} \bar{\mathbf{c}}_{\alpha\beta\gamma} \quad (14)$$

where $\bar{\mathbf{l}}_\alpha$, $\bar{\mathbf{u}}_{\alpha\beta}$ and $\bar{\mathbf{c}}_{\alpha\beta\gamma}$ represent each column vectors of the multi-dimensional tensors according to the linear, quadratic and cubic forms $\bar{\mathcal{L}}$, $\bar{\mathcal{Q}}$ and $\bar{\mathcal{C}}$, respectively. Consideration of the orthogonality constraints (8)-(10) allows to express equations (12)-(14) in terms of two augmented systems of linear equations:

$$\begin{bmatrix} \mathbf{K} & -\mathbf{F} \\ -\mathbf{F}^T & \mathbf{0} \end{bmatrix} \begin{bmatrix} \mathbf{u}_\alpha \\ \bar{\mathbf{l}}_\alpha \end{bmatrix} = \begin{bmatrix} \mathbf{0} \\ -\mathbf{e}_\alpha \end{bmatrix} \quad (15)$$

$$\begin{bmatrix} \mathbf{K} & -\mathbf{F} \\ -\mathbf{F}^T & \mathbf{0} \end{bmatrix} \begin{bmatrix} \mathbf{u}_{\alpha\beta} \\ \bar{\mathbf{u}}_{\alpha\beta} \end{bmatrix} = \begin{bmatrix} -\mathcal{Q}(\mathbf{u}_\alpha, \mathbf{u}_\beta) \\ \mathbf{0} \end{bmatrix} \quad (16)$$

and the relation:

$$\bar{\mathbf{c}}_{\alpha\beta\gamma\delta} = \mathcal{C}(\mathbf{u}_\alpha, \mathbf{u}_\beta, \mathbf{u}_\gamma, \mathbf{u}_\delta) - \frac{2}{3}[\mathbf{u}_{\alpha\beta}^T \mathcal{L}(\mathbf{u}_{\delta\gamma}) + \mathbf{u}_{\beta\gamma}^T \mathcal{L}(\mathbf{u}_{\delta\alpha}) + \mathbf{u}_{\gamma\alpha}^T \mathcal{L}(\mathbf{u}_{\delta\beta})] \quad (17)$$

in which \mathbf{K} is the $(N \times N)$ -dimensional tangent stiffness matrix at the nominal configuration, i.e. the tensor representation of the linear form \mathcal{L} , where the $(N \times (m+1))$ -dimensional matrix \mathbf{F} follows from the perturbation loads, eq. (5), and \mathbf{e}_α denotes the the α -th unit vector with coefficient $e_\alpha = 1$. The load vector $\mathcal{Q}(\mathbf{u}_\alpha, \mathbf{u}_\beta)$ is assembled from the solution of (15) with coefficients $(Q_{i\alpha\beta} u_\alpha u_\beta)$.

The solution of the augmented systems of equations for $m+1$ load vectors provides the first and second order solutions needed to construct the reduced order model. In the following we present a concise summary of the construction of the reduced order model and the global equilibrium solution. A detailed summary revealing the relations between the higher order forms of (5) and (11) and the derived systems of equations can be found in [12]:

- the tensor coefficients of the linear form $\bar{\mathcal{L}}$ are obtained from pre-multiplication of (12) with the first order solution \mathbf{u}_β and using the orthogonality condition (8):

$$\bar{\mathbf{l}}_{\alpha\beta} = \mathbf{e}_\beta^T \bar{\mathbf{l}}_\alpha = \mathbf{u}_\beta^T \mathcal{L}(\mathbf{u}_\alpha) \quad (18)$$

- the tensor coefficients of the quadratic form $\bar{\mathcal{Q}}$ are obtained from pre-multiplication of (13) with the first order solution \mathbf{u}_γ and using the orthogonality condition (9):

$$\bar{\mathbf{q}}_{\gamma\alpha\beta} = \mathbf{e}_\gamma^T \bar{\mathbf{u}}_{\alpha\beta} = \mathbf{u}_\gamma^T \mathcal{Q}(\mathbf{u}_\alpha, \mathbf{u}_\beta) \quad (19)$$

- the tensor coefficients of the cubic form $\bar{\mathcal{C}}$ are obtained from pre-multiplication of (14) with the first order solution \mathbf{u}_δ and using the orthogonality condition (10). Assuming a conservative system, the tensor of the corresponding cubic form is symmetric with coefficients:

$$\bar{\mathbf{c}}_{\alpha\beta\gamma\delta} = \mathcal{C}(\mathbf{u}_\alpha, \mathbf{u}_\beta, \mathbf{u}_\gamma, \mathbf{u}_\delta) - \frac{2}{3}(\mathbf{u}_{\alpha\beta}^T \mathcal{L}(\mathbf{u}_{\delta\gamma}) + \mathbf{u}_{\beta\gamma}^T \mathcal{L}(\mathbf{u}_{\delta\alpha}) + \mathbf{u}_{\gamma\alpha}^T \mathcal{L}(\mathbf{u}_{\delta\beta})). \quad (20)$$

where $\mathcal{C}(\mathbf{u}_\alpha, \mathbf{u}_\beta, \mathbf{u}_\gamma, \mathbf{u}_\delta) = \mathbf{u}_\delta^T \mathcal{C}(\mathbf{u}_\alpha, \mathbf{u}_\beta, \mathbf{u}_\gamma)$ depends on the first order displacement solution only.

- with the equations (18)-(20), the following reduced order model of dimension $(m + 1)$ can be established for the solution of the unknown generalized displacements ξ :

$$\bar{\mathcal{L}}(\xi) + \bar{\mathcal{Q}}(\xi, \xi) + \bar{\mathcal{C}}(\xi, \xi, \xi) = \phi = \Delta\lambda \mathbf{e}_1 \quad (21)$$

where $\Delta\lambda$ is chosen to be the load parameter of the external load \mathbf{f}_{ext} to determine the response to the actual loading and \mathbf{e}_1 is the first unit vector. Equation (21) is conveniently solved using an arc-length method [1, 28] and its solution sets the generalized displacements ξ into a non-linear relation to the actual load increment $\Delta\lambda$, which is mapped to the solution space of the total problem invoking the displacement expansion:

$$\mathbf{u} = \mathbf{u}_0 + \mathbf{u}_\alpha \xi_\alpha + \mathbf{u}_{\alpha\beta} \xi_\alpha \xi_\beta \quad (22)$$

and the actual load factor $\lambda = \lambda_0 + \Delta\lambda$.

2.2. Koiter-Newton path-following analysis

The reduced order model of the previous sub-section is based on Koiter's asymptotic expansion theory and constructed at a known configuration along the non-linear equilibrium path. The model solution, eq. (22), is used as a computationally efficient predictor in a step-by-step path-tracing analysis. Compared to a linearized predictor scheme based on a Newton-type method the pre-eminence of the Koiter predictor becomes evident due to its asymptotic solution properties towards the equilibrium path which allows for significantly larger step sizes at reduced out-of-balance forces. The latter is driven to zero using a few Newton correction steps of the full system. The step size of the reduced order model is controlled by the following criteria:

$$\frac{\|\mathbf{R}\|}{\lambda \|\mathbf{f}_{ex}\|} \geq \epsilon \quad (23)$$

where the value of ϵ is a user defined measure for an appropriate step size. The applied convergence criterion for the Newton correction in this work was chosen to be:

$$\frac{\|\mathbf{R}\|}{\lambda \|\mathbf{f}_{ex}\|} \leq 10^{-4}. \quad (24)$$

Following the work of *Riks* [1], a constraint hyperplane is adopted in order to avoid a possible loss of convergence near limit loads. Details of the Newton iteration with the *Riks* constraint can be found in [21, 19].

The construction of the reduced order model is dominated by the factorization of the governing system of equations of the augmented problem (15) and (16), respectively. It is important to note that both systems of equations of dimension $(N + m + 1)$ have an identical system matrix, hence factorization is needed only once. The number m of perturbation loads is typically small (< 10) since only modes which are closely spaced to the nominal configuration are considered. If buckling is fully absent only the external load vector becomes significant and the reduced order model degenerates to a model size of *one*. The computational effort of the correction phase requires p Newton iterations of the full system of equations to ensure sufficient stability of the scheme.

3. SOLID-SHELL CONCEPT AND MIXED FORMULATION

In the following, we derive a solid-shell element formulation within the framework of the Koiter-Newton method. The element type is an eight-node hybrid stress element proposed by *Sze* [17] and presented here using a Green-Lagrange strain measure. At first, we present a pure displacement-based solid-shell formulation which we extend in a follower step to a mixed formulation to enhance the performance of the Koiter-Newton approach in terms of an improved convergence behaviour.

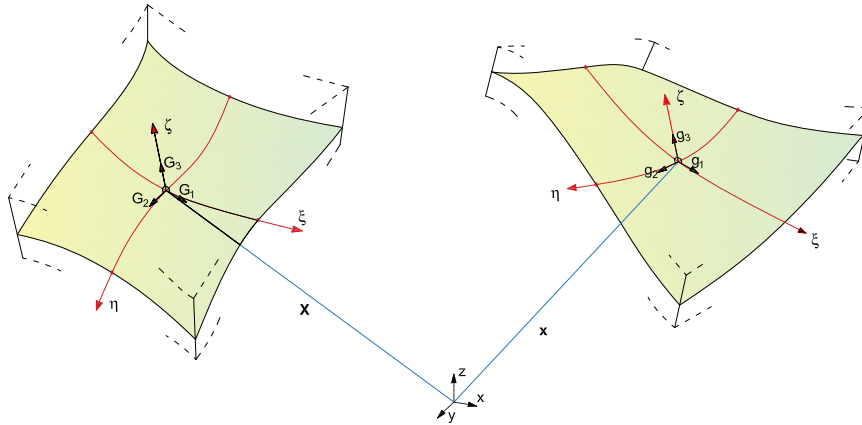


Figure 1. Undeformed and deformed shell geometry.

3.1. Displacement-based solid-shell element

Commonly, low-order shell elements are prone to locking phenomena. Here, the chosen element formulation counteracts shear locking and trapezoidal locking with an *Assumed Natural Strain (ANS)* approach and *Selective Reduced Integration (SRI)*. Furthermore, to eliminate thickness locking, an appropriate through-the-thickness normal stress assumption is introduced.

3.1.1. Kinematics We use a Total Lagrangian formulation to identify material points of the current configuration C^t in terms of their position vector $\mathbf{X}(\xi, \eta, \zeta)$ in the reference configuration C^0 and the displacement state $\mathbf{d}(\xi, \eta, \zeta)$, cf Fig. 1:

$$\mathbf{x}(\xi, \eta, \zeta) = \mathbf{X}(\xi, \eta, \zeta) + \mathbf{d}(\xi, \eta, \zeta) \quad (25)$$

where $\zeta = [\xi, \eta, \zeta]$ denote convective curvilinear shell coordinates with (ξ, η) representing in-plane coordinates and ζ being the shell thickness coordinate. The covariant basis vectors in the undeformed and deformed configuration are obtained from the corresponding partial derivatives of the position vectors \mathbf{x} and \mathbf{X} , respectively:

$$\mathbf{G}_i = \mathbf{X}_{,i}, \quad \mathbf{g}_i = \mathbf{x}_{,i} = \mathbf{G}_i + \mathbf{d}_{,i} \quad \text{with } i = 1, 2, 3, \quad (26)$$

where $(\cdot)_{,i}$ denotes the partial derivative with respect to ζ_i . The contravariant basis vectors follow from the dual basis condition: $\mathbf{g}_i \cdot \mathbf{g}^j = \mathbf{G}_i \cdot \mathbf{G}^j = \delta_i^j$ and the metric coefficients are $g_{ij} = \mathbf{g}_i \cdot \mathbf{g}_j$ and $G_{ij} = \mathbf{G}_i \cdot \mathbf{G}_j$ with $(i, j = 1, 2, 3)$. The motion of material points from the initial reference configuration C^0 to the current configuration C^t is described by the deformation map $\mathbf{F} : \mathbf{x} \rightarrow \mathbf{X}$:

$$\mathbf{F} = \frac{\partial \mathbf{x}}{\partial \mathbf{X}} = \mathbf{g}_i \otimes \mathbf{G}^i. \quad (27)$$

Using the deformation gradient (27) and the metric tensor coefficients g_{ij} and G_{ij} , the Green-Lagrange strain tensor is expressed as:

$$\mathbf{E} = \frac{1}{2}(\mathbf{F}^T \mathbf{F} - \mathbf{I}) = \bar{E}_{ij} \mathbf{G}^i \otimes \mathbf{G}^j \quad (28)$$

with

$$\bar{E}_{ij} = \frac{1}{2}(g_{ij} - G_{ij}) = \frac{1}{2}(\mathbf{G}_i \cdot \mathbf{d}_{,j} + \mathbf{d}_{,i} \cdot \mathbf{G}_j + \mathbf{d}_{,i} \cdot \mathbf{d}_{,j}) \quad (29)$$

Using a *Voigt* notation we collect the coefficients of the symmetric strain tensor in a vector $\bar{\boldsymbol{\varepsilon}} = [\bar{E}_{\xi\xi}, \bar{E}_{\eta\eta}, 2\bar{E}_{\xi\eta}, \bar{E}_{\zeta\zeta}, 2\bar{E}_{\eta\zeta}, 2\bar{E}_{\xi\zeta}]^T$.

3.1.2. *Discretization aspects* The displacements of the eight-node hexahedron shell element are interpolated using trilinear functions:

$$\mathbf{d}(\zeta) = \mathbf{N}(\zeta) \mathbf{q} \quad (30)$$

where \mathbf{q} collects the element nodal displacements and $\mathbf{N}(\zeta)$ the interpolation functions. The element geometry is interpolated with the same interpolation functions, following the isoparametric paradigm.

The discrete element formulation needs to consider additional means to ensure sufficient robustness of the low order shell element. In order to eliminate shear and trapezoidal locking, we redefine the transverse shear strain components $\bar{E}_{\eta\zeta}$, $\bar{E}_{\xi\zeta}$ and the transverse normal strain component $\bar{E}_{\zeta\zeta}$, respectively, by the *Assumed Natural Strain (ANS)* technique [29, 30] with number and location of the sampling points as reported in [17]. To this end, we assume the Z -axis and the X - Y -plane to be parallel to the ζ -axis and mid-surface of the shell, respectively. To enhance the in-plane bending response of the element, the in-plane shear strain $\bar{E}_{\xi\eta}$ is substituted by its value at $\xi = \eta = 0$ which is a *Selective Reduced Integration (SRI)* retaining the correct matrix rank.

The covariant strains are linearized with respect to ζ :

$$\bar{\boldsymbol{\varepsilon}} \approx \begin{bmatrix} \bar{\mathbf{e}}(\xi, \eta) + \zeta \bar{\boldsymbol{\chi}}(\xi, \eta) \\ \bar{E}_{\zeta\zeta}(\xi, \eta) \\ \bar{\boldsymbol{\gamma}}(\xi, \eta) \end{bmatrix} \quad (31)$$

where

$$\bar{\mathbf{e}}(\xi, \eta) = \begin{bmatrix} \bar{E}_{\xi\xi}(\xi, \eta, 0) \\ \bar{E}_{\eta\eta}(\xi, \eta, 0) \\ 2\bar{E}_{\xi\eta}(\xi, \eta, 0) \end{bmatrix} \quad \bar{\boldsymbol{\chi}}(\xi, \eta) = \begin{bmatrix} \bar{E}_{\xi\xi,\zeta}(\xi, \eta, 0) \\ \bar{E}_{\eta\eta,\zeta}(\xi, \eta, 0) \\ 2\bar{E}_{\xi\eta,\zeta}(\xi, \eta, 0) \end{bmatrix} \quad \bar{\boldsymbol{\gamma}}(\xi, \eta) = \begin{bmatrix} 2\bar{E}_{\eta\zeta}(\xi, \eta, 0) \\ 2\bar{E}_{\xi\zeta}(\xi, \eta, 0) \end{bmatrix}.$$

Finally, the generalized covariant strain components are collected in a vector and transformed into a local Cartesian basis:

$$\boldsymbol{\varepsilon}(\xi, \eta) = \mathbf{T}(\xi, \eta) \begin{bmatrix} \bar{\mathbf{e}} \\ \bar{E}_{\zeta\zeta} \\ \bar{\boldsymbol{\chi}} \\ \bar{\boldsymbol{\gamma}} \end{bmatrix} \quad (32)$$

where $\mathbf{T}(\xi, \eta)$ denotes the transformation matrix that maps the strain tensor from the covariant basis to the local Cartesian basis. The coefficients of \mathbf{T} are shown in detail in the Appendix A.

The local covariant strains are discretized using component-wise the partial derivatives of the interpolated displacements, eq. (30), and are expressed in terms of a strain interpolation matrix:

$$\boldsymbol{\varepsilon} = \mathbf{B}(\mathbf{q}) \mathbf{q} \quad \text{with} \quad \mathbf{B}(\mathbf{q}) = \mathbf{B}_L + \frac{1}{2} \mathbf{B}_Q(\mathbf{q}) \quad (33)$$

where \mathbf{B}_L and $\mathbf{B}_Q(\mathbf{q})$ denote the linear and quadratic part of the strain displacement equations (32).

3.1.3. *Statics* The second Piola-Kirchhoff stress tensor \mathbf{S} is derived from the constitutive relation using the Green-Lagrange strain tensor \mathbf{E} which follows from tensor coefficients of eq. (32):

$$\mathbf{S} = \mathbb{C} : \mathbf{E} \quad (34)$$

with \mathbb{C} being a material constitutive matrix. The generalized second Piola-Kirchhoff stresses can be written as:

$$\boldsymbol{\sigma} = \mathbb{C} \boldsymbol{\varepsilon} \quad (35)$$

using the generalized constitutive matrix \mathbf{C} which is obtained by analytic pre-integration of \mathbb{C} along ζ so that:

$$\int_{-1}^1 \int_{-1}^1 \int_{-1}^1 \mathbf{S} : \mathbf{E} \det(\mathbf{J}) d\xi d\eta d\zeta \approx \int_{\Omega^0} \boldsymbol{\varepsilon}^T \mathbf{C} \boldsymbol{\varepsilon} \quad (36)$$

where from now on, we use the simplifying notation: $\int_{\Omega^0} (\circ) = 2 \int_{-1}^1 \int_{-1}^1 (\circ) \det(\mathbf{J}(\xi, \eta, 0)) d\xi d\eta$, in which \mathbf{J} denotes the Jacobian matrix $\mathbf{J}(\xi, \eta, \zeta) = [\mathbf{G}_1, \mathbf{G}_2, \mathbf{G}_3]^T$ of the element.

The slender solid-shell element is also prone to thickness locking which is eliminated assuming the normal stress component S_{zz} to be constant through the thickness [17].

3.1.4. Displacement-element contributions to the third order form governing equations The third order form equilibrium of the Koiter-Newton method as presented in the section 2 is expressed in terms of a linear, quadratic and cubic form which are obtained in the following by differentiating the strain energy with respect to the global degrees of freedom, cf equation (2).

Notation: The quantities derived in the following refer to an element formulation if not state differently. A corresponding element indicating index notation is skipped for the sake of a better readability.

The strain energy contribution of the shell element and corresponding derivatives are:

$$U = \int_{\Omega^0} \frac{1}{2} \boldsymbol{\varepsilon}^T \mathbf{C} \boldsymbol{\varepsilon} \quad (37)$$

$$\frac{\partial U}{\partial \mathbf{q}} = \int_{\Omega^0} \tilde{\mathbf{B}}(\mathbf{q})^T \boldsymbol{\sigma}(\mathbf{q}) = \mathbf{f}^{int}(\mathbf{q}) \quad (38)$$

$$\frac{\partial^2 U}{\partial \mathbf{q}^2} = \int_{\Omega^0} \tilde{\mathbf{B}}(\mathbf{q})^T \mathbf{C} \tilde{\mathbf{B}}(\mathbf{q}) + \int_{\Omega^0} \sum_i \sigma_i(\mathbf{q}) \boldsymbol{\Gamma}_i = \mathbf{K}(\mathbf{q}) \quad (39)$$

where $\tilde{\mathbf{B}}(\mathbf{q}) = \mathbf{B}_L + \mathbf{B}_Q(\mathbf{q})$, \mathbf{K} is the element tangent stiffness matrix, cf eq. (15), \mathbf{f}^{int} represent the internal elastic element forces and

$$\boldsymbol{\sigma}(\mathbf{q}) = \mathbf{C} \mathbf{B}(\mathbf{q}) \mathbf{q} \quad (40)$$

are the generalized second Piola-Kirchhoff stresses. The matrices $\boldsymbol{\Gamma}_i$ account for the geometric element stiffness and are defined as:

$$\boldsymbol{\Gamma}_i = \frac{\partial^2 \varepsilon_i}{\partial \mathbf{q}^2}. \quad (41)$$

Furthermore, we introduce the following discrete operators to express the quadratic and cubic form of the equilibrium in a compact notation:

$$\boldsymbol{\sigma}(\mathbf{q}_\alpha, \mathbf{q}_\beta) = \mathbf{C} \tilde{\mathbf{B}}(\mathbf{q}_\alpha) \mathbf{q}_\beta \quad (42)$$

$$\boldsymbol{\sigma}_L(\mathbf{q}) = \mathbf{C} \mathbf{B}_L \mathbf{q} \quad (43)$$

$$\boldsymbol{\varepsilon}_Q(\mathbf{q}_\alpha, \mathbf{q}_\beta) = \mathbf{B}_Q(\mathbf{q}_\alpha) \mathbf{q}_\beta \quad (44)$$

$$\boldsymbol{\sigma}_Q(\mathbf{q}_\alpha, \mathbf{q}_\beta) = \mathbf{C} \boldsymbol{\varepsilon}_Q(\mathbf{q}_\alpha, \mathbf{q}_\beta). \quad (45)$$

Using (40)-(45), the following forms are derived:

Linear form The linear form is expressed in terms of the tangent properties at the known reference point with displacements \mathbf{q}_0 :

$$\mathcal{L}(\mathbf{q}_\alpha) = \mathbf{K}(\mathbf{q}_0) \mathbf{q}_\alpha. \quad (46)$$

Quadratic form The quadratic form depends linearly on the known displacement state of the reference point and mixed quadratically on the first order displacements \mathbf{q}_α and \mathbf{q}_β , respectively,

$$\begin{aligned} \mathcal{Q}(\mathbf{q}_\alpha, \mathbf{q}_\beta) &= \int_{\Omega^0} \mathbf{B}_Q(\mathbf{q}_\alpha)^T \boldsymbol{\sigma}(\mathbf{q}_0, \mathbf{q}_\beta) + \mathbf{B}_Q(\mathbf{q}_\beta)^T \boldsymbol{\sigma}(\mathbf{q}_0, \mathbf{q}_\alpha) \\ &\quad + \tilde{\mathbf{B}}(\mathbf{q}_0)^T \boldsymbol{\sigma}_Q(\mathbf{q}_\alpha, \mathbf{q}_\beta) \\ &= \mathbf{Q}(\mathbf{q}_\alpha) \mathbf{q}_\beta \end{aligned} \quad (47)$$

with

$$\mathbf{Q}(\mathbf{q}_\alpha) = \int_{\Omega^0} \mathbf{B}_Q(\mathbf{q}_\alpha)^T \mathbf{C} \tilde{\mathbf{B}}(\mathbf{q}_0) + \tilde{\mathbf{B}}(\mathbf{q}_0)^T \mathbf{C} \mathbf{B}_Q(\mathbf{q}_\alpha) + \sum_i \sigma_i(\mathbf{q}_0, \mathbf{q}_\alpha) \boldsymbol{\Gamma}_i. \quad (48)$$

Cubic form Finally, the cubic form follows as:

$$\begin{aligned} \mathcal{C}(\mathbf{q}_\alpha, \mathbf{q}_\beta, \mathbf{q}_\gamma, \mathbf{q}_\delta) &= \int_{\Omega^0} \{ \boldsymbol{\sigma}_Q(\mathbf{q}_\alpha, \mathbf{q}_\beta)^T \boldsymbol{\varepsilon}_Q(\mathbf{q}_\gamma, \mathbf{q}_\delta) + \boldsymbol{\sigma}_Q(\mathbf{q}_\alpha, \mathbf{q}_\gamma)^T \boldsymbol{\varepsilon}_Q(\mathbf{q}_\beta, \mathbf{q}_\delta) \\ &\quad + \boldsymbol{\sigma}_Q(\mathbf{q}_\alpha, \mathbf{q}_\delta)^T \boldsymbol{\varepsilon}_Q(\mathbf{q}_\gamma, \mathbf{q}_\beta) \}. \end{aligned} \quad (49)$$

Denoting the path tangent in $(\lambda_0, \mathbf{q}_0)$ with \mathbf{q}_λ , the geometrical stiffness matrix of the element is:

$$\mathbf{K}_\sigma = \int_{\Omega} \sum_i \sigma_{Li}(\mathbf{q}_\lambda) \boldsymbol{\Gamma}_i \quad (50)$$

where terms related to $\mathbf{B}_Q(\mathbf{q}_\lambda)$ in $\mathbf{Q}(\mathbf{q}_\lambda)$ are neglected as usual in displacement-based linearized buckling analysis, so obtaining a robust eigenvalue analysis as discussed in [31].

It is worth to note the following unique features of the derived model with impact to the solution properties:

- the model is purely displacement-based using displacement degrees of freedom only
- the strain energy has a 4th order dependence on the displacement degrees of freedom
- the Green-Lagrange strain measure is geometrically exact for a solid model
- the expanded non-linear equilibrium, eq. (4), is exact with any truncation error .

3.2. Mixed solid-shell element

In this sub-section we extend the solid-shell element to a mixed formulation. To this end, we introduce generalized contravariant second Piola-Kirchhoff stress resultants and collect the various contributions in a vector:

$$\bar{\boldsymbol{\sigma}} = [\bar{\mathcal{N}}, \bar{s}_{\zeta\zeta}, \bar{\mathcal{M}}, \bar{\mathcal{T}}]^T \quad (51)$$

where $\bar{\mathcal{N}}$ collects the normal stress resultants, $\bar{s}_{\zeta\zeta}$ is the stress resultant orthogonal the shell surface, $\bar{\mathcal{M}}$ represents the moment stress resultants and where $\bar{\mathcal{T}}$ assembles the transverse shear stress resultants:

$$\bar{\mathcal{N}} = \frac{1}{2} \int_{-1}^1 \bar{\boldsymbol{\sigma}}_p d\zeta \quad \bar{\mathcal{M}} = \frac{1}{2} \int_{-1}^1 \zeta \bar{\boldsymbol{\sigma}}_p d\zeta \quad (52)$$

$$\bar{s}_{\zeta\zeta} = \frac{1}{2} \int_{-1}^1 \bar{S}_{\zeta\zeta} d\zeta \quad \bar{\mathcal{T}} = \frac{1}{2} \int_{-1}^1 \bar{\boldsymbol{\tau}} d\zeta \quad (53)$$

with the stress components:

$$\bar{\boldsymbol{\sigma}}_p = \begin{bmatrix} \bar{S}_{\xi\xi} \\ \bar{S}_{\eta\eta} \\ \bar{S}_{\xi\eta} \end{bmatrix} \quad \bar{\boldsymbol{\tau}} = \begin{bmatrix} \bar{S}_{\xi\zeta} \\ \bar{S}_{\eta\zeta} \end{bmatrix}. \quad (54)$$

The generalized contravariant stresses are interpolated using an *optimal* interpolation approach [17], similar to the model proposed by *Pian* [32]:

$$\bar{\boldsymbol{\sigma}}(\xi, \eta) = \bar{\mathbf{N}}_{\sigma}(\xi, \eta) \boldsymbol{\beta} \quad (55)$$

where $\boldsymbol{\beta}$ collects the 18 discrete stress degrees of freedom of the element and $\bar{\mathbf{N}}_{\sigma}(\xi, \eta)$ contains the 18 stress interpolation functions, accordingly, as explicitly reported in [10]. Finally the generalized Cartesian stresses are transformed into the local Cartesian coordinate system:

$$\boldsymbol{\sigma}(\boldsymbol{\beta}) = \mathbf{T}^{-T}(0, 0) \bar{\boldsymbol{\sigma}} = \mathbf{N}_{\sigma} \boldsymbol{\beta} \quad (56)$$

where the matrix \mathbf{T} , cf Appendix A, is evaluated at $\xi = 0, \eta = 0$ to preserve a constant stress state. The element vector of degrees of freedom is now extended by the unknowns $\boldsymbol{\beta}$:

$$\mathbf{u} = \begin{bmatrix} \boldsymbol{\beta} \\ \mathbf{q} \end{bmatrix} \quad (57)$$

and all further algebraic element quantities are split accordingly. Following the principle of *Hellinger-Reissner* [32] the strain energy expression can be rewritten in mixed form as:

$$U_M(\mathbf{u}) = \int_{\Omega^0} \boldsymbol{\sigma}^T \boldsymbol{\varepsilon} - \frac{1}{2} \boldsymbol{\sigma}^T \mathbf{C}^{-1} \boldsymbol{\sigma} \quad (58)$$

where the subscript M indicates the mixed formulation.

Here, it is important to note that the independent interpolation of the stresses allow to reduce the order of the polynomial dependence of the strain energy on the discrete degrees of freedom, resulting in $\boldsymbol{\sigma}$ being linear in $\boldsymbol{\beta}$ and $\boldsymbol{\varepsilon}$ being quadratic in \mathbf{q} .

3.2.1. Mixed-element contributions to the third order form governing equations The mixed internal force vector of the element is

$$\mathbf{s}_M(\mathbf{u}) = \begin{bmatrix} \mathbf{s}_{\beta} \\ \mathbf{s}_q \end{bmatrix} \quad (59)$$

with

$$\mathbf{s}_{\beta} = \int_{\Omega^0} \mathbf{N}_{\sigma}^T (\boldsymbol{\varepsilon}(\mathbf{q}) - \mathbf{C}^{-1} \boldsymbol{\sigma}(\boldsymbol{\beta})) \quad (60)$$

$$\mathbf{s}_q = \int_{\Omega^0} \tilde{\mathbf{B}}(\mathbf{q})^T \boldsymbol{\sigma}(\boldsymbol{\beta}) \quad (61)$$

and the mixed element stiffness matrix is:

$$\mathbf{K}_M[\mathbf{u}] = \begin{bmatrix} \mathbf{K}_{\beta\beta} & \mathbf{K}_{\beta q}(\mathbf{q}) \\ \mathbf{K}_{\beta d}(\mathbf{q})^T & \mathbf{K}_{qq}(\boldsymbol{\beta}) \end{bmatrix} \quad (62)$$

with

$$\mathbf{K}_{\beta\beta} = - \int_{\Omega^0} \mathbf{N}_{\sigma}^T \mathbf{C}^{-1} \mathbf{N}_{\sigma} \quad (63)$$

$$\mathbf{K}_{\beta q}(\mathbf{q}) = \int_{\Omega^0} \mathbf{N}_{\sigma}^T \tilde{\mathbf{B}}(\mathbf{q}) \quad (64)$$

$$\mathbf{K}_{qq}(\boldsymbol{\beta}) = \int_{\Omega^0} \sum_i \sigma_i(\boldsymbol{\beta}) \boldsymbol{\Gamma}_i \quad (65)$$

which are evaluated as the gradient and the Hessian of the strain energy, respectively.

The linear, quadratic and cubic form of the Koiter-Newton equilibrium equations follow in analogy to the displacement formulation of 3.1:

$$\mathcal{L}_M(\mathbf{u}_\alpha) = \mathbf{K}_M(\mathbf{u}_0) \mathbf{u}_\alpha \quad (66)$$

$$\mathcal{Q}_M(\mathbf{u}_\alpha, \mathbf{u}_\beta) = \begin{bmatrix} \mathcal{Q}_\beta(\mathbf{q}_\alpha, \mathbf{q}_\beta) \\ \mathcal{Q}_q(\mathbf{u}_\alpha, \mathbf{u}_\beta) \end{bmatrix} \quad (67)$$

with

$$\mathcal{Q}_\beta(\mathbf{u}_\alpha, \mathbf{u}_\beta) = \int_{\Omega^0} \mathbf{N}_\sigma^T \varepsilon_Q(\mathbf{q}_\alpha, \mathbf{q}_\beta) \quad (68)$$

$$\mathcal{Q}_q(\mathbf{u}_\alpha, \mathbf{u}_\beta) = \int_{\Omega^0} \mathbf{B}_Q(\mathbf{q}_\alpha)^T \boldsymbol{\sigma}(\boldsymbol{\beta}_\beta) + \mathbf{B}_Q(\mathbf{q}_\beta)^T \boldsymbol{\sigma}(\boldsymbol{\beta}_\alpha) \quad (69)$$

The geometric stiffness matrix of the element is evaluated as

$$\mathbf{K}_\sigma(\boldsymbol{\beta}_\lambda) = \begin{bmatrix} \mathbf{0} & \mathbf{0} \\ \mathbf{0} & \mathbf{K}_{\sigma qq}(\boldsymbol{\beta}_\lambda) \end{bmatrix} \quad (70)$$

with

$$\mathbf{K}_{\sigma qq}(\boldsymbol{\beta}_\lambda) = \int_{\Omega^0} \sum_i \sigma_i(\boldsymbol{\beta}_\lambda) \boldsymbol{\Gamma}_i. \quad (71)$$

Finally, we note that the cubic form simplifies with:

$$\mathcal{C}_M(\mathbf{u}_\alpha, \mathbf{u}_\beta, \mathbf{u}_\gamma, \mathbf{u}_\delta) = 0 \quad (72)$$

which is a consequence of the introduced stress variables. The variables are independent and condensed out on element level before assembly, thus not increasing the global number of equations. The condensation steps are shown in detail in Appendix B.

4. NUMERICAL TESTS

In this section, we consider various numerical tests with regard to buckling of thin-walled structures to study the performance of the proposed mixed solid-shell element within the framework of the Koiter-Newton method. In particular, we will demonstrate the numerical performance in terms of convergence measures compared to pure displacement-based formulations. The chosen examples include a benchmark test of a U-shape thin-walled beam under compression to verify the overall concept and a modified thin-walled beam structure from engineering. The equilibrium paths of both structures show a distinct non-linear behavior but a minor affinity to global buckling. With a thin cylinder structure we demonstrate the method's ability to trace reliably snap-back behavior. Finally, we have selected a thin-walled frame structure to reveal the reliability of the method in presence of bifurcation after a strong non-linear pre-critical behavior.

The Koiter-Newton method reconstructs the equilibrium path evaluating just a few true equilibrium points. The solution between two consecutive points can be recovered exploiting the asymptotic reduced-order model predictor.

4.1. U-shape cantilever beam

The U-shaped cantilever beam considered here is a standard benchmark problem to verify the non-linear properties of the method, including local buckling phenomena [21]. Nevertheless, the problem is a severe test case for the Koiter-Newton approach due to a distinct non-linear pre-critical behavior which must be represented in the reduced order model by the degree of freedom associated with the

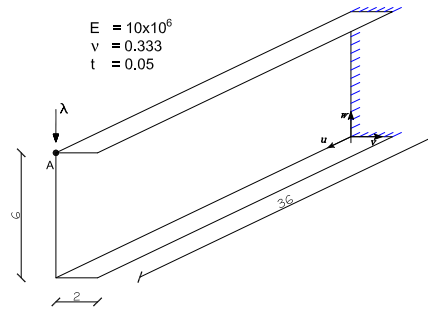


Figure 2. U-shape cantilever beam: model properties.

external load. The geometry, the material properties and boundary conditions are depicted in Fig. 2. The cantilever beam is subjected to an end shear force.

The analysis result in terms of solution steps along the equilibrium path is shown in Fig. 3. The path was fully traced within 5 Koiter-Newton steps. We selected the first 4 buckling modes which, together with the external load, ended in a reduced order model of dimension 5. Both, the mixed and the displacement-based version show virtually identical results.

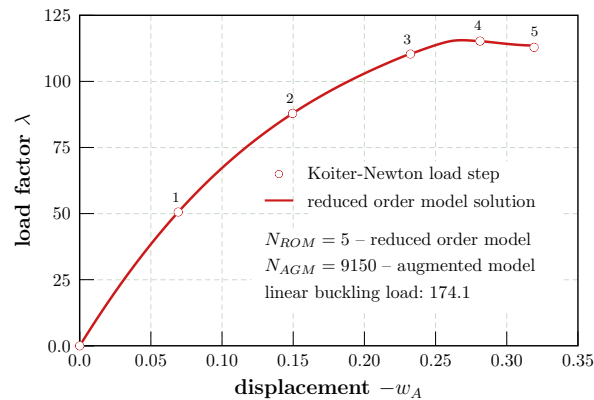


Figure 3. U-shape cantilever beam: equilibrium path with Koiter-Newton steps.

The asymptotic character of the Koiter-Newton predictor followed closely the non-linear equilibrium path. Still, an average number of 5 Newton iterations were necessary for the displacement-based solution to recover equilibrium at a sufficient accuracy level. In Tab. I we compare the corrector effort of the two approaches, the solution-based and the mixed model. The results clearly reveal a superiority of mixed model which needed on average less than 3 Newton iterations to provide equilibrium of equivalent accuracy. Recalling the dominance of the corrector phase in the complexity analysis of the Koiter-Newton method and keeping in mind that the construction of the reduced order model is computationally cheaper for the mixed model avoiding the evaluation of the third order form, this improvement is quite encouraging with regard to larger problems.

In Figures 4 and 5, the first and the second mode used to construct the reduced order model at the reference configuration and at the equilibrium point 3, respectively, are depicted. The distinct non-linear pre-critical path entails essential changes of the relevant modes along the equilibrium path which requires a repeated construction of the reduced order model to capture reliably the limit point and any post-critical behaviour. This is confirmed, regarding the deformed configuration at the

	displacement	mixed
step 1	3	2
step 2	5	3
step 3	4	3
step 4	5	2
step 5	8	4
total	25	14

Table I. U-shape beam: number of Newton iterations in the corrector phase.

equilibrium point 4, which is well represented by the modes of the reduced order model, evaluated at 3.

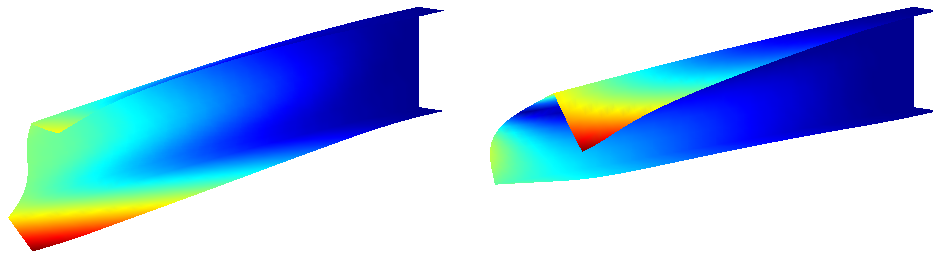


Figure 4. U-shape cantilever beam: first mode (left) and second mode (right) of the *reduced order model* constructed at the reference configuration.

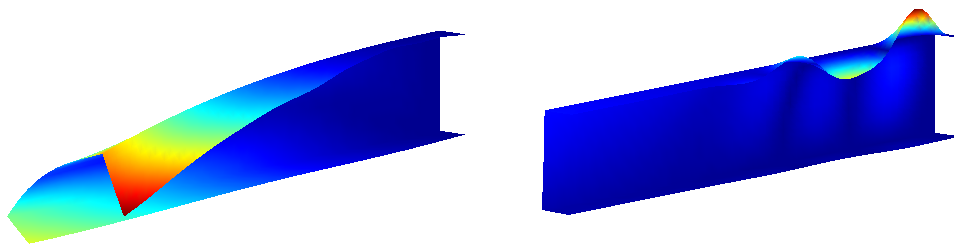


Figure 5. U-shape cantilever beam: first mode (left) and second mode (right) of the *reduced order model* constructed at 3.

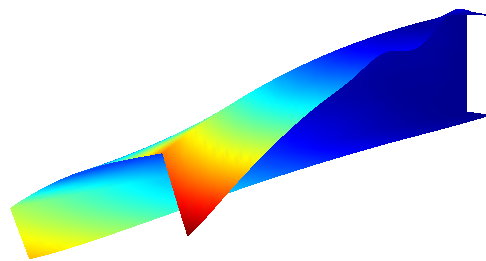


Figure 6. U-shape cantilever beam: deformed configuration (scale factor 10) at 4.

4.2. Lipped channel column

Next, we consider a lipped channel column modeled as thin-walled structure under pressure load. The geometry, material properties and loads are shown in Fig. 7. The cross-sectional in-plane displacements were constrained at both ends. The model is a perfect representative of structures with global-local buckling interaction [33] leading to a high imperfection sensitivity and had been studied previously in [34].

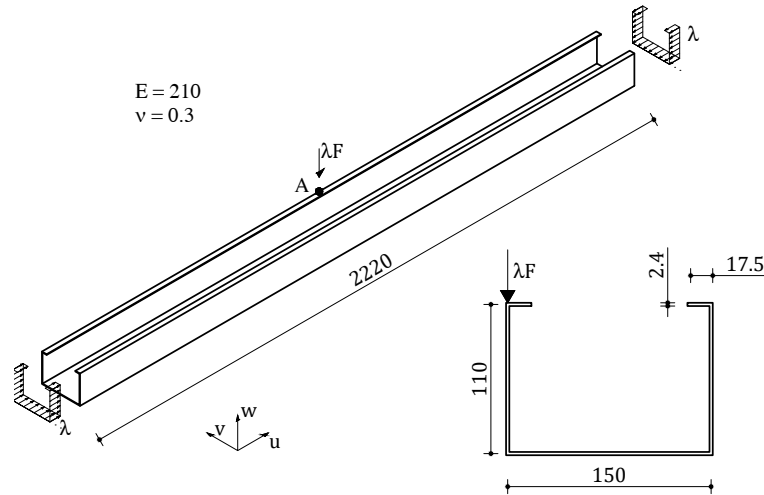


Figure 7. Lipped channel column: model properties.

The structure was analysed with 4 different amplitudes of the imperfection load to study the column's sensitivity properties. The analysis results for the different imperfection loads are depicted in Fig. 8 in which P denotes the cross-section perimeter, showing highly varying limit loads. The corresponding reduced order model of each analysis was constructed from 4 buckling modes adopting 3 Koiter-Newton steps to trace the complete equilibrium path. In Tab. II, the number of Newton iterations of the corrector phase for the mixed and the displacement-based approach is reported. Again a reduction of the computational effort of more than 30% was observed. Compared to the results of 4.1 the gain in computational efficiency using the mixed model has slightly dropped but still is very clearly visible and indicates a superior performance.

	displacement	mixed
step 1	3	2
step 2	3	2
step 3	3	2
total	9	6

Table II. Lipped channel column: number of Newton iterations in the corrector phase.

The evolution of the deformed configuration along the equilibrium path is depicted in Fig. 9. A combination of torsional and local buckling is clearly visible.

4.3. Laminate composite cylinder subjected to axial compression

Cylinder buckling is a severe numerical test case for non-linear solution methods since a pronounced snap-back behavior must be reliably captured with strongly degrading algebraic properties of the governing system of equations. Nevertheless, a steadily growing tendency to use

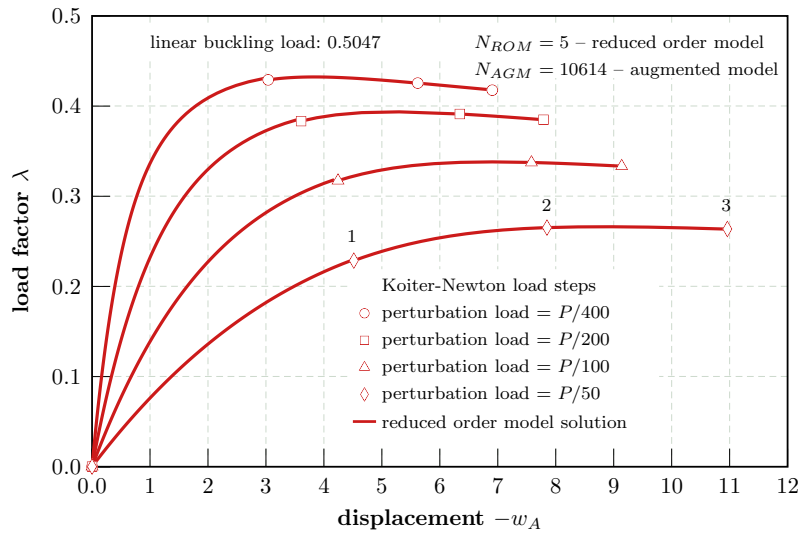


Figure 8. Lipped channel column: equilibrium paths for different perturbation loads.

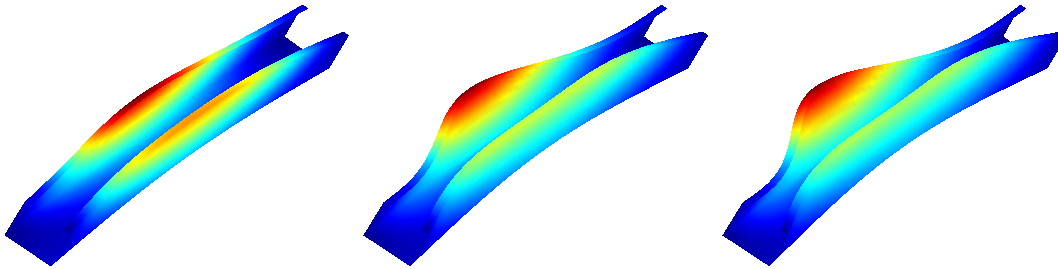


Figure 9. Lipped channel column: deformed configurations (scale factor 10) at 1, 2 and 3.

laminated composite cylindrical structures as primary structures in aerospace engineering and other lightweight engineering disciplines emphasizes the importance of a highly reliable, accurate and computationally efficient prognosis of stability properties.

The cylinder considered in the following and labelled Z33 and was manufactured and tested by DLR (German Aerospace Center) and is commonly used as validation model for numerical developments in the context of laminated composite shell design [35, 36]. The laminate stacking sequence is $in[0/0/19/-19/37/-37/45/-45/51/-51]_{out}$ with the angles measured from the cylinder axis with respect to the outward normal. The cylinder has a height of 510, a radius of $R = 250$ and a wall-thickness of $t = 1.25$, cf Fig. 10. The ply properties are $E_1 = 123.6$, $E_2 = E_3 = 8.7$, $\nu_{12} = 0.32$, $\nu_{13} = \nu_{23} = 0$, $G_{12} = G_{13} = G_{23} = 5.7$.

The cylinder model is clamped at the bottom face and has a pinned support in radial direction at the top. A uniformly distributed load along the top rim was applied in axial direction. A geometric imperfection was introduced by a single perturbation load halfway up the cylinder axis. The end-shortening result was measured at a single node of the cylinder's top rim, labelled as displacement u_A .

The complete equilibrium path was traced with 7 Koiter-Newton steps, cf Fig. 11. As common for compressed cylinders, the elastic response is characterized by an almost linear pre-critical path, followed by a bifurcation and snap-back behaviour. The cylinder problem demonstrates the ability of the non-linear Koiter predictor to capture accurately the bifurcation point, which is a potential

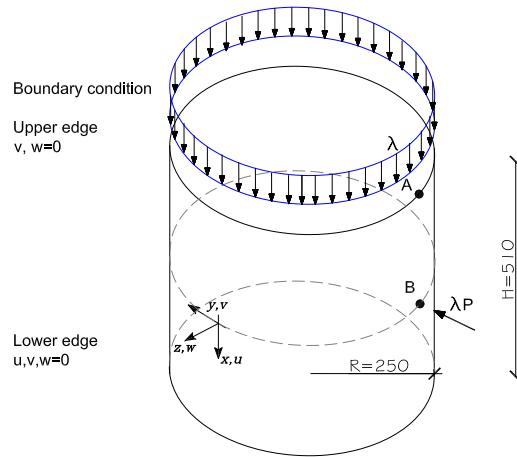


Figure 10. Laminate composite cylinder: model properties.

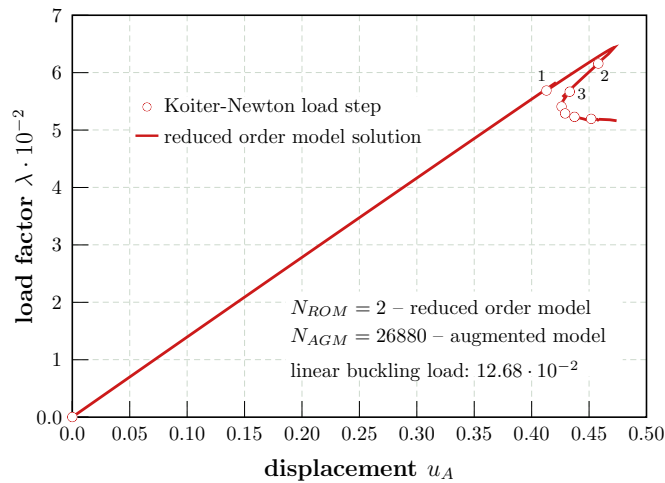


Figure 11. Laminate composite cylinder: equilibrium path.

failure mode for standard arc-length techniques with linear predictor, unless a very small step size is used.

The constructed reduced order model used only a single buckling mode in addition to the path tangent. The first and the second mode used to construct the reduced order model at the undeformed configuration and at the equilibrium point 1, respectively, are depicted in Figs. 12 and 13. From Fig. 14 it can be seen that the modes change along the equilibrium path due to the applied imperfection load. As a consequence, a repeated reconstruction of the reduced order model was required to capture accurately the bifurcation and the post-critical deformation.

Finally, the number of Newton iterations during the corrector phase are reported in Tab. III. Interestingly, the gain of computational efficiency using the mixed approach is very moderate compared to the pure displacement formulation which can be mainly attributed to an already extremely good performance of the displacement-based Koiter-Newton model which is more than four times less compared to standard Newton-based method [14].

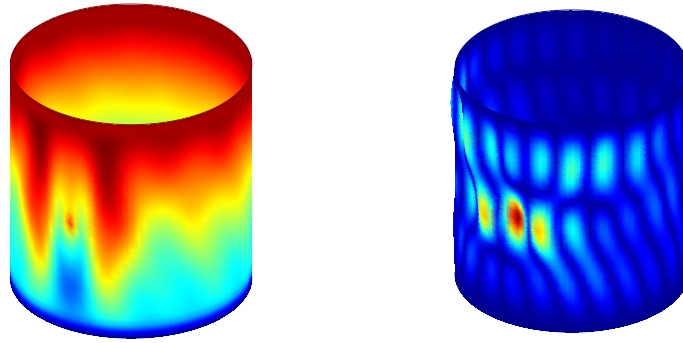


Figure 12. Laminate composite cylinder: first and second modes of the *reduced order model* at the reference configuration.

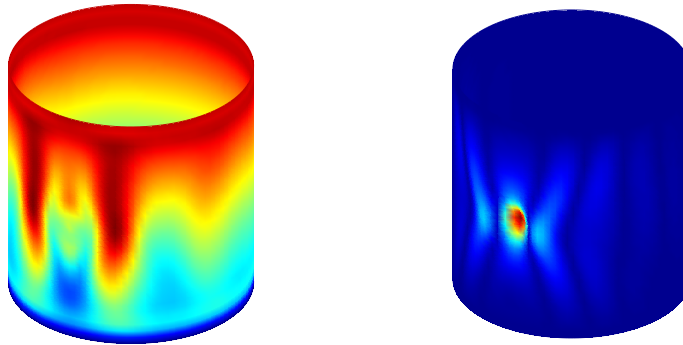


Figure 13. Laminate composite cylinder: first and second mode of the *reduced order model* at 1.

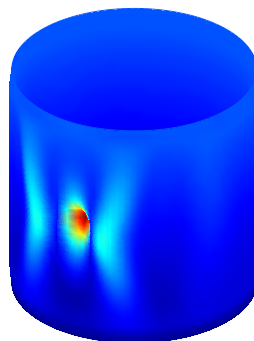


Figure 14. Laminate composite cylinder: deformed configuration (scale factor 25) at 2

4.4. Thin-walled frame

Finally, we choose a thin-walled frame structure which undergoes a distinct non-linear deformation with a bifurcation in the pre-critical path [11]. The geometry and boundary conditions are illustrated in Fig. 15. The material properties are $E = 3.10275$ and $\nu = 0.3$.

The equilibrium path is depicted in Fig. 16 which is characterised by the bifurcation along a non-linear pre-critical path due to a local buckling near the clamped section. This can be seen from the evolution of the deformed configuration shown in Fig. 17.

	displacement	mixed
step 1	3	2
step 2	2	2
step 3	2	2
step 4	2	2
step 5	2	2
step 6	2	2
step 7	3	2
total	16	14

Table III. Laminate composite cylinder: number of Newton iterations in the corrector phase.

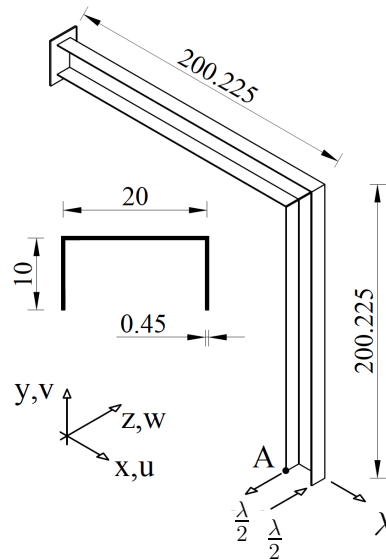


Figure 15. Thin-walled frame: model properties.

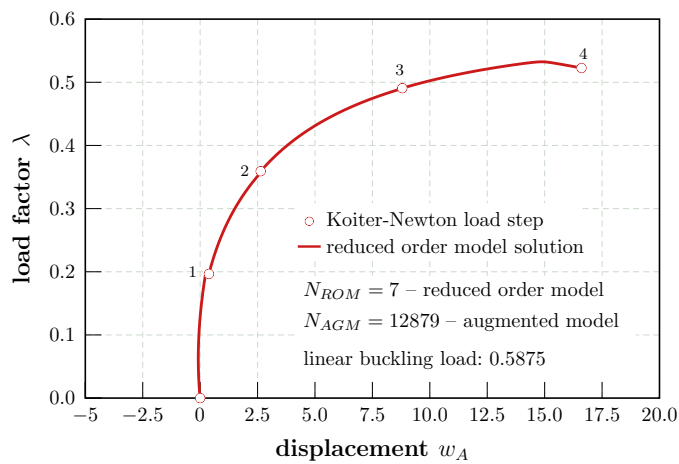


Figure 16. Thin-walled frame: equilibrium path.

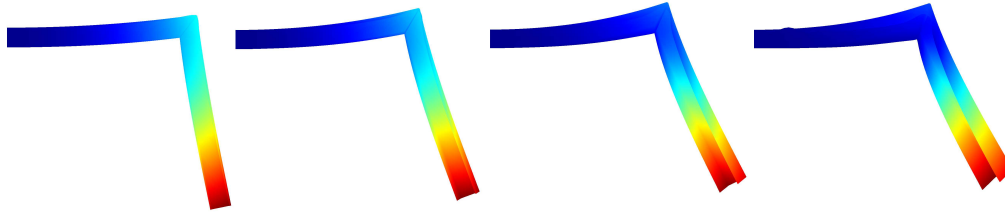


Figure 17. Thin-walled frame: evolution of the deformed configuration (scale factor 15).

The Koiter-Newton analysis was carried out with 4 steps using a reduced order model which was constructed on the basis of the first 6 buckling modes. Again, the proposed mixed formulation shows a significant improvement in terms of Newton iterations which reduce by more than 40% compared to the conventional model, cf Tab. IV.

	displacement	mixed
step 1	4	2
step 2	3	2
step 3	4	2
step 4	3	2
total	14	8

Table IV. Thin-walled frame: number of iterations required.

5. SUMMARY, CONCLUSIONS & OUTLOOK

In this paper, we explored the performance properties of a mixed model formulation in the framework of the recently introduced Koiter-Newton method which is a reduced order model approach for geometric non-linear analyses with an emphasis on buckling failure of thin-walled structures. In this context, a solid shell model was formulated following the Hellinger-Reissner variational principle which proved to be highly beneficial towards the computational efficiency of the analysis. The Koiter-Newton method is a step-by-step equilibrium path tracing approach which exploits the asymptotic expansion properties of Koiter's post-buckling theory in the predictor phase while mapping the solution space to a reduced order model. The construction of the reduced order model is based on the expansion of the elastic inner forces at a known state of equilibrium using the path tangent and a few closely spaced linear buckling modes, thus exciting bifurcating branches of the equilibrium path. In general, the expansion applies derivatives of the strain energy up to the fourth order which requires the evaluation of linear, quadratic and cubic forms during the construction of the reduced order model. Using a mixed model, as favoured in this work, the cubic form vanishes due to independently behaving degrees of freedom representing the unknown stress resultants on element level with beneficial consequences in terms of computational efficiency.

Here, we have started with a compact presentation of the Koiter-Newton approach to set the necessary terminology, to reveal the principal characteristics and aspects of the method. We then introduced a displacement based solid shell element which was extended in a follower step to a mixed formulation. The element formulation can be summarized highlighting the following features:

- the element is an eight-node solid element using a trilinear interpolation approach with a Green-Lagrange strain measure. This basic element type was chosen to facilitate the extension to a mixed formulation and to keep the algebraic expressions of the higher order forms simple.

In this context a future extension to a high-order element formulation [37, 38, 39] will be a reasonable extension to profit from a higher order approximation quality of the involved displacement derivatives,

- an *Assumed Natural Strain* approach was used in combination with a selective reduced integration strategy to counteract the element's affinity to locking. Furthermore, thickness locking was prevented by a constant normal stress assumption, both being well established techniques which have proven stability and reliability in low-order element formulations where high slenderness may lead to a loss of mechanical performance. Again, a future extension to a higher order approximation scheme which may remove any locking by order elevation promises to be a significant improvement in terms of stability and accuracy,
- in the mixed element formulation additional unknown stress degrees of freedom were introduced. The variables are independent of adjacent elements and thus can be eliminated on system level by an element-wise static condensation. The third order form vanishes in the mixed formulation thus simplifying and economizing the expensive contribution to the construction of the reduced order model.

The proposed formulation was tested with several numerical tests and compared to the conventional Koiter-Newton method which, in a number of studies [12, 14, 15], has already proven a superior performance compared to classical path-tracing technologies. The asymptotic Koiter predictor towards the equilibrium path allows for significantly increased step sizes such that the full path often can be traced within a few steps, revealing all neuralgic points along the path, including limit and branching points. Furthermore, a snap-back and snap-through behavior as common in the analysis of thin shells and slender structures is reliably captured and makes the approach a robust technology for stability analyses. The real strength of the proposed formulation was revealed with the corrector phase in each step which uses Newton iterations on the full system to drive the force residual below the chosen accuracy level and therefore represents numerically the most expensive part of the analysis. We have shown that the novel approach can significantly reduce the number of iterations, partly by more than 50% and even in presence of bifurcation and for very large step sizes of problems which showed highly non-linear deformation properties in the pre-critical range. In all tested cases we observed an average number of *two* Newton iterations to regain equilibrium. Compared to traditional methods, both versions, the displacement based approach and the mixed model approach, demonstrated their superiority in terms of using only a fraction of the numerical effort which is also reflected in a corresponding time efficiency, cf [13, 16].

We believe that the proposed Koiter-Newton approach is an essential extension of the conventional approach towards a reliable and robust non-linear analysis tool for thin-walled structures, in particular when buckling is the dominant physical phenomenon. We see a strong relevance of such methods in the systematic analysis of the various types of imperfections in shell buckling which often requires the consideration of a large number of test cases in deterministic and stochastic studies. The mixed model formulation should be extended in future work to more sophisticated element types which exploit higher order approximation properties and will be able to further enhance the analysis quality in terms of accuracy and continuity of the elastic buckling response of geometric imperfect structures.

Acknowledgments: The first author gratefully acknowledges the support from the School of Engineering, University of Glasgow, during his six months research stay at Glasgow.

Appendix A. Strain tensor transformation from co-variant to Cartesian coordinates

The generalized coefficients of the covariant strain tensor, eq. (32) of sub-section 3.1.1, are transformed into the local Cartesian coordinate system with the transformation matrix:

$$\mathbf{T}[\xi, \eta] = \begin{bmatrix} \mathbf{T}_p & 0 & 0 & 0 \\ 0 & T_z & 0 & 0 \\ 0 & 0 & \mathbf{T}_p & 0 \\ 0 & 0 & 0 & \mathbf{T}_t \end{bmatrix}$$

where the sub-matrices are:

$$\begin{aligned} T_z &= 1/J_{33}^2 \\ \mathbf{T}_p &= \begin{bmatrix} J_{11}^2 & J_{12}^2 & 2J_{11}J_{12} \\ J_{21}^2 & J_{22}^2 & 2J_{21}J_{22} \\ J_{21}J_{11} & J_{22}J_{12} & J_{22}J_{11} + J_{21}J_{12} \end{bmatrix}^{-T} \\ \mathbf{T}_t &= \begin{bmatrix} J_{12}J_{33} + J_{13}J_{32} & J_{13}J_{31} + J_{11}J_{33} \\ J_{22}J_{33} + J_{23}J_{32} & J_{23}J_{31} + J_{21}J_{33} \end{bmatrix}^{-T}. \end{aligned}$$

and where \mathbf{J} denotes the Jacobian matrix.

Appendix B. Static condensation for the governing element equations

The introduction of independent unknown stress coefficients in sub-section 3.2 provides a natural split of the governing element equations of the mixed formulation:

$$\begin{bmatrix} \mathbf{K}_{\beta\beta} & \mathbf{K}_{\beta q} \\ \mathbf{K}_{\beta q}^T & \mathbf{K}_{qq} \end{bmatrix} \begin{bmatrix} \boldsymbol{\beta} \\ \mathbf{q} \end{bmatrix} = \begin{bmatrix} \mathbf{f}_\beta \\ \mathbf{f}_q \end{bmatrix}$$

which allows a static condensation of the stress coefficients $\boldsymbol{\beta}$:

$$\begin{aligned} \boldsymbol{\beta} &= \mathbf{K}_{\beta\beta}^{-1} \mathbf{f}_\beta - \mathbf{K}_{\beta\beta}^{-1} \mathbf{K}_{\beta q} \mathbf{q} \\ -\mathbf{K}_{\beta q}^T \mathbf{K}_{\beta\beta}^{-1} \mathbf{K}_{\beta q} \mathbf{q} &= \mathbf{f}_q - \mathbf{K}_{\beta q}^T \mathbf{K}_{\beta\beta}^{-1} \mathbf{f}_\beta \end{aligned}$$

which results in the condensed relation:

$$\mathbf{K}_c \mathbf{q} = \mathbf{f}_c$$

where

$$\begin{aligned} \mathbf{K}_c &= -\mathbf{K}_{\beta q}^T \mathbf{K}_{\beta\beta}^{-1} \mathbf{K}_{\beta q} \\ \mathbf{f}_c &= \mathbf{f}_q - \mathbf{K}_{\beta q}^T \mathbf{K}_{\beta\beta}^{-1} \mathbf{f}_\beta. \end{aligned}$$

Similarly, for the linear buckling equations follows:

$$\begin{bmatrix} \mathbf{K}_{\beta\beta} & \mathbf{K}_{\beta q} \\ \mathbf{K}_{\beta q}^T & \mathbf{K}_{qq} \end{bmatrix} \begin{bmatrix} \boldsymbol{\beta} \\ \mathbf{q} \end{bmatrix} + \lambda \begin{bmatrix} \mathbf{0} & \mathbf{0} \\ \mathbf{0} & \mathbf{K}_{\sigma qq} \end{bmatrix} \begin{bmatrix} \boldsymbol{\beta} \\ \mathbf{q} \end{bmatrix} = \mathbf{0}$$

with

$$\begin{aligned} \mathbf{K}_c \mathbf{q} + \lambda \mathbf{K}_{\sigma qq} \mathbf{q} &= \mathbf{0} \\ \boldsymbol{\beta} &= -\mathbf{K}_{\beta\beta}^{-1} \mathbf{K}_{\beta q} \mathbf{q}. \end{aligned}$$

References

1. Riks E. An incremental approach to the solution of snapping and buckling problems. *International Journal of Solids and Structures* 1979; **15**(7):529–551, doi:10.1016/0020-7683(79)90081-7.
2. Koiter W. On the stability of elastic equilibrium. PhD Thesis.
3. Lanzo AD, Garcea G, Casciaro R. Asymptotic post-buckling analysis of rectangular plates by hc finite elements. *International Journal for Numerical Methods in Engineering* 1995; **38**(14):2325–2345.
4. Rahman T, Jansen E. Finite element based coupled mode initial post-buckling analysis of a composite cylindrical shell. *Thin-Walled Structures* 2010; **48**(1):25–32, doi:10.1016/j.tws.2009.08.003.

5. Flores F, Godoy L. Elastic post-buckling analysis via finite element and perturbation techniques. Part I: Formulation. *International Journal for Numerical Methods in Engineering* 1992; **33**(9):1775–1794.
6. Boutyour E, Zahrouni H, Potier-Ferry M, Boudi M. Asymptotic-numerical method for buckling analysis of shell structures with large rotations. *Journal of Computational and Applied Mathematics* 2004; **168**(1-2):77–85, doi: 10.1016/j.cam.2003.05.010.
7. Silvestre N, Camotim D. Asymptotic-numerical method to analyze the postbuckling behavior, imperfection-sensitivity, and mode interaction in frames. *Journal of Engineering Mechanics* 2005; **131**(6):617–632, doi: 10.1061/(ASCE)0733-9399(2005)131:6(617).
8. Chen H, Virgin L. Finite element analysis of post-buckling dynamics in plates-Part I: An asymptotic approach. *International Journal of Solids and Structures* 2006; **43**(13):3983–4007, doi:10.1016/j.ijsolstr.2005.04.036.
9. Garcea G, Leonetti L, Magisano D, Gonçalves R, Camotim D. Deformation modes for the post-critical analysis of thin-walled compressed members by a Koiter semi-analytic approach. *International Journal of Solids and Structures* 2017; **110-111**:367–384, doi:10.1016/j.ijsolstr.2016.09.010.
10. Magisano D, Leonetti L, Garcea G. Koiter asymptotic analysis of multilayered composite structures using mixed solid-shell finite elements. *Composite Structures* 2016; **154**:296–308, doi:10.1016/j.compstruct.2016.07.046.
11. Garcea G, Liguori F, Leonetti L, Magisano D, Madeo A. Accurate and efficient a-posteriori account of geometrical imperfections in Koiter finite element analysis. *International Journal for Numerical Methods in Engineering* 2017; doi:10.1002/nme.5550.
12. Liang K, Abdalla M, Gürdal Z. A Koiter-Newton approach for nonlinear structural analysis. *International Journal for Numerical Methods in Engineering* 2013; **96**(12):763–786, doi:10.1002/nme.4581.
13. Liang K, Ruess M, Abdalla M. The Koiter-Newton approach using von Karman kinematics for buckling analyses of imperfection sensitive structures. *Computer Methods in Applied Mechanics and Engineering* 2014; **279**:440–468, doi:10.1016/j.cma.2014.07.008.
14. Liang K, Ruess M. Nonlinear buckling analysis of the conical and cylindrical shells using the SGL strain based reduced order model and the PHC method. *Aerospace Science and Technology* 2016; **55**:103–110.
15. Liang K, Ruess M, Abdalla M. Co-rotational finite element formulation used in the Koiter-Newton method for nonlinear buckling analyses. *Finite Elements in Analysis and Design* 2016; **116**:38–54.
16. Liang K, Ruess M, Abdalla M. An eigenanalysis-based bifurcation indicator proposed in the framework of a reduced-order modeling technique for non-linear structural analysis. *International Journal of Non-Linear Mechanics* 2016; **81**:129–138, doi:10.1016/j.ijnonlinmec.2016.01.013.
17. Sze K, Chan W, Pian T. An eight-node hybrid-stress solid-shell element for geometric non-linear analysis of elastic shells. *International Journal for Numerical Methods in Engineering* 2002; **55**(7):853–878, doi:10.1002/nme.535.
18. Klinkel S, Gruttmann F, Wagner W. A robust non-linear solid shell element based on a mixed variational formulation. *Computer Methods in Applied Mechanics and Engineering* 2006; **195**(1-3):179–201, doi: 10.1016/j.cma.2005.01.013.
19. Garcea G, Trunfio G, Casciaro R. Mixed formulation and locking in path-following nonlinear analysis. *Computer Methods in Applied Mechanics and Engineering* 1998; **165**(1-4):247–272.
20. Magisano D, Leonetti L, Garcea G. Advantages of the mixed format in geometrically nonlinear analysis of beams and shells using solid finite elements. *International Journal for Numerical Methods in Engineering* 2016; doi: 10.1002/nme.5322.
21. Magisano D, Leonetti L, Garcea G. How to improve efficiency and robustness of the newton method in geometrically non-linear structural problem discretized via displacement-based finite elements. *Computer Methods in Applied Mechanics and Engineering* 2017; **313**:986–1005, doi:http://dx.doi.org/10.1016/j.cma.2016.10.023.
22. Garcea G, Madeo A, Casciaro R. Nonlinear FEM analysis for beams and plate assemblages based on the implicit corotational method. *J. Mech. Mater. Struct.* 2012; **7**(6):539–574, doi:10.2140/jomms.2012.7.539.
23. Garcea G, Madeo A, Zagari G, Casciaro R. Asymptotic post-buckling FEM analysis using corotational formulation. *International Journal of Solids and Structures* 2009; **46**(2):377–397.
24. Zagari G, Madeo A, Casciaro R, De Miranda S, Ubertini F. Koiter analysis of folded structures using a corotational approach. *International Journal of Solids and Structures* 2013; **50**(5):755–765, doi:10.1016/j.ijsolstr.2012.11.007.
25. Klinkel S, Gruttmann F, Wagner W. Continuum based three-dimensional shell element for laminated structures. *Computers and Structures* 1999; **71**(1):43–62, doi:10.1016/S0045-7949(98)00222-3.
26. Argyris J. An excursion into large rotations. *Computer Methods in Applied Mechanics and Engineering* 1982; **32**:85–155, doi:10.1002/nme.5322.
27. Aklonis M, Goldberger V. *Tensor Calculus with Applications*. World Scientific Publishing Co. Pte. Ltd.: Singapore, 2003.
28. Belytschko T, Liu W, Moran B. *Nonlinear Finite Elements for Continua and Structures*. John Wiley Sons, Ltd: Chichester, 2000.
29. Bischoff M, Ramm E. Shear deformable shell elements for large strains and rotations. *International Journal for Numerical Methods in Engineering* 1997; **40**:4427–4449.
30. Schwarze M, Reese S. A reduced integration solid-shell finite element based on the EAS and the ANS concept - Geometrically linear problems. *International Journal for Numerical Methods in Engineering* 2009; **80**:1322–1355.
31. Garcea G, Salerno G, Casciaro R. Extrapolation locking and its sanitization in Koiter's asymptotic analysis. *Computer Methods in Applied Mechanics and Engineering* 1999; **180**(1-2):137–167.
32. Pian THH, Wu CC. *Hybrid and Incompatible Finite Element Methods*. Chapman & All, CRC: New-York, 1969.
33. Garcea G, Gonçalves R, Bilotta A, Manta D, Bebiano R, Leonetti L, Magisano D, Camotim D. Deformation modes of thin-walled members: A comparison between the method of Generalized Eigenvectors and Generalized Beam Theory. *Thin-Walled Structures* 2016; **100**:192–212, doi:10.1016/j.tws.2015.11.013.
34. Post-buckling behaviour and strength of cold-formed steel lipped channel columns experiencing distortional/global interaction. *Computers & Structures* 2011; **89**(3-4):422–434, doi:http://doi.org/10.1016/j.compstruc.2010.11.015.
35. Zagari G, Zucco G, Madeo A, Ungureanu V, Zinno R, Dubina D. Evaluation of the erosion of critical buckling load of cold-formed steel members in compression based on Koiter asymptotic analysis. *Thin-Walled Structures* 2016;

- 108**:193–204, doi:10.1016/j.tws.2016.08.011.
36. Castro SG, Zimmermann R, Arbelo MA, Degenhardt R. Exploring the constancy of the global buckling load after a critical geometric imperfection level in thin-walled cylindrical shells for less conservative knock-down factors. *Thin-Walled Structures* 2013; **72**:76–87, doi:http://dx.doi.org/10.1016/j.tws.2013.06.016.
 37. Hosseini S, Remmers J, Verhoosel C, de Borst R. An isogeometric continuum shell element for non-linear analysis. *Computer Methods in Applied Mechanics and Engineering* 2014; **271**:1–22.
 38. Düster A, Bröker H, Rank E. The p-version of the finite element method for three-dimensional curved thin walled structures. *International Journal for Numerical Methods in Engineering* 2001; **52**:673–703.
 39. Rank E, Ruess M, Kollmannsberger S, Schillinger D, Düster A. Geometric modeling, isogeometric analysis and the finite cell method. *Computer Methods in Applied Mechanics and Engineering* 2012; **249-252**:104–115.